ChemPubSoc Europe
DOI: 10.1002/cctc.201901441
CHEMCATCHEM Full Papers

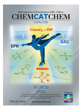

# Impact of Al Activators on Structure and Catalytic Performance of Cr Catalysts in Homogeneous Ethylene Oligomerization – A Multitechnique *in situ/operando* Study

Reni Grauke,[a] Rahel Schepper,[b] Jabor Rabeah,[a] Roland Schoch,[b] Ursula Bentrup,[a] Matthias Bauer,*[b] and Angelika Brückner*[a, c]

The effect of different $AlR_3$ activators (R = methyl, ethyl, isobutyl, n-octyl) has been studied in comparison to modified methylaluminoxane (MMAO) by *operando* EPR as well as by *in situ* UV-vis, ATR-IR and XANES/EXAFS spectroscopy during oligomerization of ethylene at 20 bar and 40 °C with a homogeneous Cr complex catalyst formed *in situ* upon mixing a $Cr(acac)_3$ precursor, a $Ph_2PN(^iPr)PPh_2$ ligand (PNP) and the activator. Coordination of PNP to $Cr(acac)_3$ is initiated only in the presence of an activator. Highest 1-octene productivity (detected during *operando* EPR measurements) was obtained with MMAO which promotes bidentate coordination of the ligand to form an active $(PNP)Cr^{II}(CH_3)_2$ chelate complex. Rising bulkiness of R in $AlR_3$ leads to only monodentate coordination of PNP to the Cr center by one P atom and increasing reduction to $Cr^I$ to a maximum extend of around 30% for $AlOct_3$. This lowers the catalytic performance, which is mainly governed by the mode of PNP coordination rather than by the $Cr^I$ content.

## Introduction

Linear $\alpha$-olefins (LAOs) such as 1-hexene or 1-octene serve as co-monomers in the production of linear low-density polyethylene (LLDPE), as detergents, synthetic lubricants and plasticizers.[1] Almost half of world's LAO demand is produced by the Shell higher olefin oligomerization process (SHOP).[2] The disadvantage of this process is a statistical so-called Schulz-Flory distribution of olefins with different chain length that often do not meet the market demand and have to be separated by energy-intensive fractionation. For the production of olefins with specific chain length, much effort has been dedicated to selective oligomerization to save energy and process costs. Comprehensive investigations during the last 20 years revealed that selective ethylene oligomerization leading preferentially to 1-hexene and/or 1-octene is possible with organochromium complexes in the presence of an alkyl aluminum co-catalyst.[3] Initially, these catalytic systems were optimized for ethylene trimerization and the respective state of the art has been reviewed by Dixon et al. in 2004.[4] In the same year, a breakthrough in ethylene tetramerization was achieved using Cr complexes with bidentate diphosphinoamine (PNP = $Ph_2PN(R)PPh_2$) ligands activated by modified methylaluminoxane (MMAO).[3e] These systems provided 1-octene selectivities of up to 70 %. Since then many efforts have been made and still continue, to optimize the catalytic activity and 1-octene selectivity by varying ligands and reaction conditions.[5]

Generally, the active catalyst in selective ethylene tri- and tetramerization is formed *in situ* by mixing solutions of a Cr precursor (e.g. $Cr(acac)_3$, $CrCl_3(THF)_3$, $CrCl_2$), the respective ligand and an aluminum containing co-catalyst such as methylaluminoxane (MAO), modified MAO (MMAO), ethylaluminoxane (EAO), *iso*-butylaluminoxane (*i*-BAO) or alkyl aluminum compounds ($AlR_3$). Frequently, the role of the activator is considered to cause alkylation of the Cr center followed by alkide abstraction and formation of an ion pair with a cationic Cr complex.[4,6]

Most of the studies of activator effects were conducted with preformed Cr complexes containing ligands that catalyze preferentially ethylene trimerization (e.g. ligands with a SNS backbone)[7] while such investigations on catalysts with PNP ligands suitable for tetramerization are rather rare. One of the few examples for the latter case comprises a preformed binuclear $Cr^{III}$-PNP complex that was treated with $AlMe_3$, yet not in the presence of ethylene, forming a heterobimetallic species

[a] R. Grauke, Dr. J. Rabeah, Dr. U. Bentrup, Prof. A. Brückner
Leibniz-Institut für Katalyse e. V. an der Universität Rostock (LIKAT)
Albert-Einstein-Str. 29a
Rostock 18059 (Germany)
E-mail: angelika.brueckner@catalysis.de
[b] Dr. R. Schepper, Dr. R. Schoch, Prof. M. Bauer
Department Chemie and Center for Sustainable Systems Design (CSSD)
Universität Paderborn
Warburger Straße 100
Paderborn D-33098 (Germany)
E-mail: matthias.bauer@upb.de
[c] Prof. A. Brückner
Department Life, Light & Matter
Faculty for Interdisciplinary Research
University of Rostock
Albert-Einstein-Straße 25
Rostock 18059 (Germany)

Supporting information for this article is available on the WWW under https://doi.org/10.1002/cctc.201901441

*This publication is part of a Special Collection on "Advanced Microscopy and Spectroscopy for Catalysis".* Please check the ChemCatChem homepage for more articles in the collection.

containing $Cr^{II}$.[8] It has also been observed that aluminum activators change the Cr valence state of the complexes in different ways, depending on their own nature. Thus, $Cr^{III}$ in a preformed $CrCl_3$(SNS) complex was reduced to $Cr^{II}$ in the presence of *i*-BAO while it remains trivalent upon interaction with both $AlEt_2Cl$ as well as $AlMe_3$.[9] This was explained by the higher propensity of *i*-butyl to undergo reductive elimination events. In our previous study we found by *operando* EPR and *in situ* XAS measurements that an active (PNP)$Cr^{II}(CH_3)_2$ complex is formed *in situ* when MMAO was used as activator.[10]

Deriving a clear correlation between the used aluminum activator and the 1-octene productivity by comparing literature results is almost impossible, since other important reaction conditions such as temperature, pressure, solvent and/or Cr precursor were different as well.[11] Moreover, conclusions on the effect of the activator in the open literature are almost exclusively based on analysis of complexes isolated from the reaction mixture after treatment of well-defined Cr complexes or of mixtures of a Cr precursor and the ligand with the Al co-catalyst in the absence of ethylene. This means that the isolated and characterized species could be different from those formed under real reaction conditions and, thus, the derived mechanistic conclusions may be of limited relevance.

Against this background, it is the aim of the present work to explore the impact of different activators with alkyl aluminum moieties on activity, selectivity and nature of the active Cr complex in ethylene oligomerization. To obtain reliable and comparable results, the same $Cr(acac)_3$ precursor and $Ph_2PN(^iPr)PPh_2$ ligand were used to form the active Cr complex *in situ* under the same reaction conditions. $AlR_3$ activators with R being methyl, ethyl, *iso*-butyl and n-octyl have been studied in comparison to MMAO. The structure of the latter is rather undefined since it is manufactured by controlled hydrolysis of a mixture of $AlR_3$ with R=methyl and *iso*-butyl, but it is usually employed in the industrial oligomerization process. For deriving reliable structure-reactivity relationships, complementary spectroscopic techniques such as electron paramagnetic resonance (EPR), ultraviolet-visible (UV-vis), attenuated total reflection-infrared (ATR-IR) and X-Ray absorption spectroscopy (XAS) have been used in *in situ* and/or *operando* mode.

## Experimental Section

All experiments were performed in the absence of air and moisture using a standard glove box and/or Schlenk technique. $Cr(acac)_3$, cyclohexane (degassed and dried over molecular sieve), 1,1-diphenyl-2-picrylhydrazyl (DPPH), alkyl aluminum compounds $AlMe_3$ (2.0 M in heptane), $AlEt_3$ and $Al^iBu_3$ (both 1.0 M in hexane), $AlOct_3$ (25 wt.% in hexane) were purchased from Sigma-Aldrich. MMAO-3 A (7 wt.% Al in heptane) was obtained from Akzo Nobel and stored at 4 °C. The $Ph_2PN(^iPr)PPh_2$ ligand (PNP) was prepared as described elsewhere[12] and kept under argon in the glove box. Ethylene (LINDE) was dried and deoxygenated by passing through a water- and oxygen trap.

Solutions of 1.25 mmol $Cr(acac)_3$ and 1.25 mmol PNP were prepared in a glove box by dissolving 6.5 mg $Cr(acac)_3$ and 8 mg of the PNP ligand in 15 mL dry cyclohexane. A standard solution of DPPH was prepared by dissolving 2 mg DPPH in 25 mL dry cyclohexane and stored at 4 °C when not used for the measurements.

### EPR Measurements

EPR measurements were performed with an EMXnano continuous wave (cw)-EPR spectrometer (Bruker) in X-Band at a microwave frequency and power of ≈9 GHz and 6.3 mW, a modulation frequency of 100 kHz and a modulation amplitude up to 8 G. For recording *operando* EPR spectra during reaction, a home-made thick-wall quartz tube reactor connected to a gas circulation system (Warnow Hydraulik) with an ethylene reservoir was directly implemented in the cavity of the spectrometer as described elsewhere.[10] Ethylene was continuously bubbled at a pressure of 20 bar *via* a capillary into the reaction solution.

For each experiment, 200 μL of the 1.25 mM $Cr(acac)_3$/PNP solution was filled into the EPR reactor. Subsequently 200 equiv. of the activator were added, the tube was tightly closed and connected to the gas circulation system. After three cycles of flushing with dry argon/evacuation, the reactor was pressurized with ethylene to 20 bar and heated to 40 °C. EPR spectra were recorded as a function of time during reaction which was stopped after 30 minutes. Ethylene conversion was determined from the pressure drop in the reservoir. After depressurizing, the reaction solution was quenched with a few drops of 10% HCl and 0.5 mL of the organic phase was transferred into a vial containing 100 μL heptane (as internal standard) and 0.7 mL cyclohexane or toluene for GC product analysis by a GC-FID (Agilent) equipped with a 19091 J-433HP-5 5% Phenyl Methyl Silox column.

To assess the reducing ability of the activator, 200 μL of the 1.25 mM $Cr(acac)_3$/PNP solution was placed in a normal EPR tube and measured at room temperature. Subsequently, 200 equiv. of the activator were added and the $Cr^{III}$ signal was measured after immediate cooling to 100 K. Thereafter, the sample was heated to room temperature and the $Cr^{I}$ signal was recorded after different times. For the determination of the $Cr^{I}$ concentration, the sample was placed in a rectangular double cavity and measured together with a DPPH standard solution performed in an ELEXYS 500 cw-EPR spectrometer (Bruker) in X-band with a microwave power of 6.3 mW, a modulation frequency of 100 kHz and modulation amplitude of up to 5 G. During the measurements the EPR cavity was continuously flushed with $N_2$ to prevent $H_2O$ condensation. The $Cr^{I}$ concentration was calculated by Equation (1), in which A is the area of the EPR signals determined by double integration.

$$c_{Cr^{+}} = \frac{A_{Cr^{+}}}{A_{DPPH}} c_{DPPH} \quad (1)$$

### UV-vis Measurements

UV-vis spectra were recorded by a fiberoptical spectrometer with a probe consisting of a quartz fiber (AvaSpec-2048, Avantes) in a special Schlenk vessel under argon after three times argon purging/evacuation to $10^{-4}$ mbar. The vessel was filled with 3 mL dry cyclohexane and then $Cr(acac)_3$ and PNP were added gradually until complete dissolution to form a 1.25 mM solution of both. 1 mL of the respective activator was diluted by 5 ml dry cyclohexane and 100 μL of this was added to the $Cr(acac)_3$/PNP solution. Spectra were recorded as a function of time at room temperature.

### IR Measurements

ATR-IR spectra were recorded between 3000–620 $cm^{-1}$ by a ReactIR 15 spectrometer equipped with a fiberoptical diamond probe (Mettler Toledo). A similar Schlenk vessel and purging procedure as for the UV-vis measurements was applied. 3 mg $Cr(acac)_3$ was added to 1 mL dry cyclohexane and heated up to 50 °C, to ensure a sufficiently high concentration, due to the limited solubility of the components at room temperature. Then 3.5 mg PNP was added until complete dissolution. 0.65 mL of the respective activator was added stepwise in portions of 0.05 mL, 0.2 mL and 0.4 mL to the $Cr(acac)_3$/PNP solution. ATR-IR spectra were recorded before and after addition of activator and as a function of time.

### XAS Measurements

XAS measurements were performed at beamline P65 at DESY-PETRA III (Deutsches Elektronen-Synchrotron) in Hamburg (Germany). The synchrotron beam current was 100 mA at 6 GeV storage ring energy. For the measurements at the chromium K-edge (5989 eV) a Si(111) double crystal monochromator was used. Energy calibration was performed with a chromium foil. The *in situ* measurements were performed in fluorescence mode with a Canberra 7 element hyper pure Ge detector. Solid reference samples were diluted in boron nitride and pressed into self-supporting wafers. All measurements of liquid samples were performed in a specially designed sample cell, which allows measurements under inert atmosphere. This cell can be evacuated and flushed with argon prior to the measurements and, additionally, it allows stirring of the solution during the collection of the spectra. Prior to the XAS measurements, the different systems were tested for the maximum allowed concentration, since the activator influences the solubility. According to these tests, different concentrations of $Cr(acac)_3$/PNP (1:1) were solved in dried cyclohexane, namely 1.25 mM for measurements with $Cr(acac)_3$/PNP/MMAO, 3.75 mM for $Cr(acac)_3/PNP/AlMe_3$, 5.0 mM for $Cr(acac)_3/PNP/AlEt_3$ and $Cr(acac)_3/PNP/Al^iBu_3$ and 10.0 mM for $Cr(acac)_3/PNP/AlOct_3$. Due to the low concentrations, self-absorption effects can be excluded. The solutions were transferred to the cell under Schlenk conditions and 200 equiv. of the respective activator were added under stirring. The solutions were allowed to equilibrate for 10 min prior to the measurements. A single scan required 20 minutes. Depending on the concentration, for all samples 5 to 10 spectra were collected and merged to obtain a better signal to noise ratio and to match the time frame of the EPR measurements. The scans were checked carefully to exclude changes before merging.

EXAFS data analysis started with background absorption removal from the experimental absorption spectrum by subtracting a Victoreen-type polynomial.[13] The third maximum of the first derivative was set as $E_0$ for the EXAFS analysis to ensure a good comparability between all systems. Afterwards the smooth part of the spectrum, corrected for pre-edge absorption, was determined by use of a piecewise polynomial which was adapted in a way that the low-R components of the resulting Fourier transform were minimal. The background subtracted spectrum was divided by its smooth part and then the photon energy was converted to photoelectron wavenumbers *k*. To avoid mistakes during the fit procedure the resulting $\chi(k)$ was weighted with $k=1$–3 and Fourier transformed using a Hanning function window. According to the curved wave formalism, data analysis was performed in *k*-space using the EXCURV98[14] program which calculates the EXAFS functions according to a formulation in terms of radial distribution functions [Eq. (2)]:

$$\chi(k) = \sum_j S_0^2(k) F_j(k) \int P_j(r_j) \frac{e^{-2r_j/\lambda}}{kr_j^2} \sin\left[2kr_j + \delta_j(k)\right] dr_j \qquad (2)$$

To calculate the theoretical spectra, XALPHA phase and amplitude functions[14] were used and the mean free path of the scattered electrons was calculated from the imaginary part of the potential (VPI set to −4.00). Additionally, a correction for the inner potential $E_f$ was introduced to adjust the phase differences of the experimental and theoretical EXAFS functions. Fitting was carried out in the range $\Delta k = 3$–10.5 $Å^{-1}$ in the range of $\Delta R = 1$–4 Å, resulting in a number of independent parameters of 16 according to a conservative reading of the Nyquist criterion.[15]

The quality of the applied least-square fit is determined by the *R*-factor, which represents the percentage disagreement between experiment and theory and takes into account systematic and random errors according to[15b,16] [Eq. (3)]

$$R = \sum_i^N \frac{k_i^n}{\sum_j^N k_j^n \mid \chi_j^{exp}(k_j)\mid} \left|\chi^{exp}(k_i) - \chi^{theo}(k_i)\right| \cdot 100\,\% \qquad (3)$$

The accuracy of the determined distances is 1%, of the Debye-Waller-like factor 10 % and of the coordination numbers depending of the distance 5–15%.[17] The amplitude reduction factor was determined to 0.8 with $Cr(acac)_3$ as reference compound.

## Results and Discussion

### *Operando* EPR Measurements

Our previous *operando* EPR and *in situ* XAS measurements of the $Cr(acac)_3$/PNP/MMAO system revealed the formation of a $(PNP)Cr^{II}(CH_3)_2$ complex immediately after mixing the three components, which is regarded as active species for ethylene conversion.[10] This went along with reduction of the EPR active $Cr^{III}$ to EPR silent $Cr^{II}$. However, a new EPR signal of low-spin $Cr^{I}$ ($S=1/2$) appeared in these experiments, the intensity of which increased with decreasing activity. Therefore, it has been assigned to an inactive Cr species. Such $Cr^{I}$ signals are also observed in the *operando* EPR spectra of Figure 1. They are split into two features arising from a $Cr^{I}$ species with ($g=2.0017$) and without a coordinated PNP ligand ($g=1.998$).[10,18] The corresponding catalytic data derived from the EPR reactor are listed in Table 1.

**Table 1.** Total $Cr^{I}$ percentage, ethylene consumption and productivity of $1\text{-}C_8H_{16}$ and $1\text{-}C_6H_{12}$ measured after 30 min reaction time.[a]

| Activator | $S_{C<6}$ [%] | $S_{1\text{-Hexene}}$ [%] | $S_{1\text{-Octene}}$ [%] | $Cr^{I}$ [%] | Consumption [$g_{Ethen}/g_{Cr}$/h] |
|---|---|---|---|---|---|
| MMAO | 22 | 13 | 65 | 2 | 60326 |
| $AlMe_3$ | 100 | 0 | 0 | 0.5 | 25441 |
| $AlEt_3$ | 66 | 34 | 0 | 15 | 32710 |
| $Al^iBu_3$ | 75 | 23 | 2 | 28 | 29075 |
| $AlOct_3$ | 51 | 17 | 32 | 30 | 39979 |

[a] General reaction conditions: $Cr(acac)_3$: 1.25 mmol, PNP – ligand: 1.25 mmol, activator: 200 equiv., solvent: cyclohexane, 20 bar ethylene, 40°–45° C, 200 μL reaction-solution.

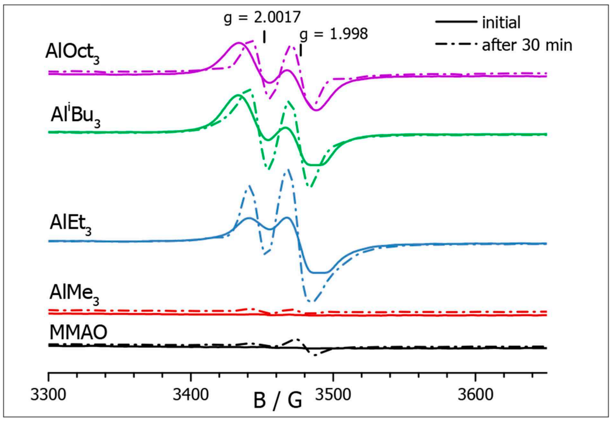


**Figure 1.** *Operando* EPR spectra of Cr(acac)3/PNP in cyclohexane with different activators measured right after adding the activator and after 30 min.

Best catalytic performance was obtained with MMAO. This agrees with the fact that only a very small signal of catalytically inactive $Cr^{I}$ was measured, amounting to only 2% of the total Cr content (Figure 1). Based on our previous study[10] it can be anticipated that the PNP ligand is properly coordinated to the Cr center, which has been found to suppress reduction to $Cr^{I}$ and promote 1-octene selectivity.[3e,5d,19] Surprisingly, even less $Cr^{I}$ has been detected, when $AlMe_3$ was used as activator, though in this case only about half of the ethylene conversion was reached and only short-chain products were formed. This is in agreement with previous observations for $AlMe_3$.[5b,20] A much higher amount of 15% $Cr^{I}$ was formed in the case of $AlEt_3$ and this increased again to 28 and 30% with $Al^{i}Bu_3$ and $AlOct_3$, respectively, though similar ethylene conversions were obtained. With these three activators, it is 1-octene selectivity that makes the difference, being zero for $AlEt_3$ but 32% for $AlOct_3$ (Table 1). It is also evident that the EPR signal of PNP-coordinated $Cr^{I}$ at $g = 2.0017$ gains intensity from $AlEt_3$ to $AlOct_3$ while it is negligible for MMAO. To elucidate the reasons for this different behavior, *in situ* studies with UV-vis, ATR-IR and X-ray absorption spectroscopy have been performed, which are described in the following sections.

### *In situ* UV-vis Measurements

Due to limitations of the experimental setup, UV-vis measurements could not be performed in operando mode. The aim was just to study the in situ-formation of the catalyst from precursors before starting the reaction. The UV-vis spectrum of $Cr(acac)_3$ in cyclohexane shows bands at 38433 $cm^{-1}$ from an intra-ligand transition and at 29677 $cm^{-1}$ from a ligand-to-metal charge transfer (LMCT) transition (Figure 2a).[21] The weak band at 25929 $cm^{-1}$ is due to a d-d transition of $Cr^{III}$.[21–22] When the PNP ligand is added to this solution, absorption at low wavenumbers increases. Comparison with the spectrum of PNP alone shows that this is just due to a superposition of the band of the free PNP ligand at 39146 $cm^{-1}$. The PNP ligand thus does not coordinate to the Cr center under these conditions. This changes, however, when an activator is added to the $Cr(acac)_3$/PNP solution (Figure 2b). In this case an immediate color change from light purple to yellowish-brown is observed, suggesting the formation of $Cr^{II}$.[22b] When MMAO is added to the $Cr(acac)_3$/PNP solution, the initial LMCT band of $Cr(acac)_3$ disappears and a new LMCT band rises at 30752 $cm^{-1}$. This is due to a change of the Cr coordination environment originating most probably from replacement of $[acac]^{-}$ by PNP and/or $CH_3$ group(s) of MMAO. This is in agreement with our previous results, which have shown that a $(PNP)Cr^{II}(CH_3)_2$ species is formed when MMAO is added to a mixed solution of $Cr(acac)_3$ and PNP in cyclohexane. When $AlMe_3$ instead of MMAO is added, an intense and broad band appears around 30752 $cm^{-1}$ and absorbance increases in the range of the free PNP ligand. $AlMe_3$ is known to be a very effective methylation agent,[23] which could lead to fast and complete methylation of the Cr center, thus hindering coordination of PNP, as evidenced by EXAFS results (*vide infra*). With $Al^{i}Bu_3$ the band at 30752 $cm^{-1}$ is

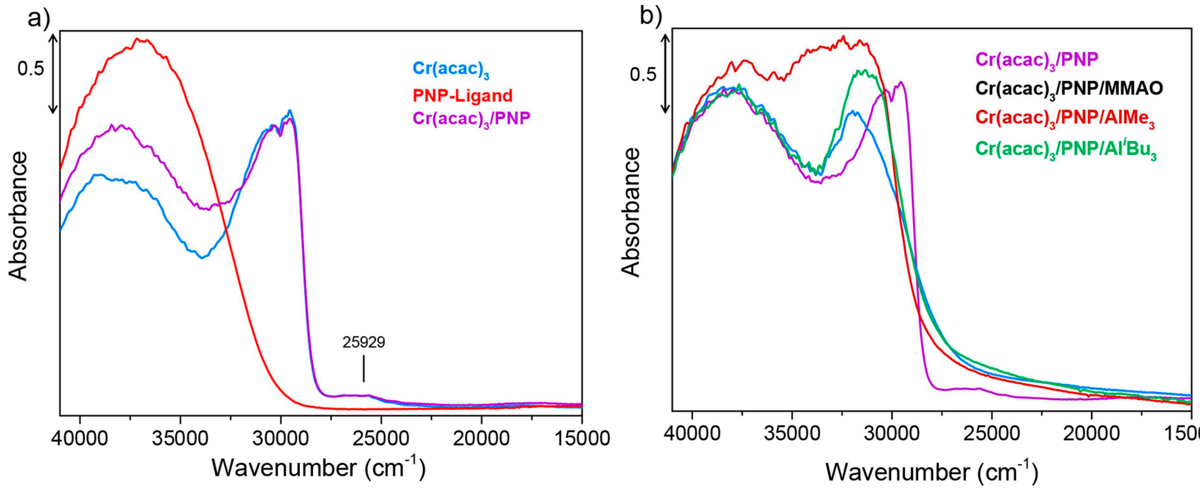


**Figure 2.** *In situ* UV-vis spectra in cyclohexane of a) $Cr(acac)_3$ before and after adding PNP ligand and b) $Cr(acac)_3$/PNP with different activators.

much less pronounced and still shows a small shoulder at 29677 $cm^{-1}$ from the $[acac]^-$ ligand. The reason may be that $Al^iBu_3$ hinders alkylation and proper coordination of PNP to the Cr center, meaning that $[acac]^-$ remains partly coordinated at Cr, as suggested by XANES data (*vide infra*). This facilitates further reduction to $Cr^I$, in agreement with the more intense EPR signal at g = 2.0017 for $Cr^I$ without coordinated PNP (Figure 1).

From EPR and UV-vis results it is evident that both techniques have intrinsic limitations. EPR can only detect low spin $Cr^I$ species while valence states with an even number of electrons such as $Cr^{II}$ and $Cr^{IV}$ are detectable, if at all, only at very low temperature, usually below 77 K. UV-vis spectroscopy just suggests an interaction of the ligand with the chromium precursor when the activator is added, yet the precise Cr coordination is not accessible. Thus, to obtain more detailed information on changes of the Cr valence state and coordination environment upon addition of the different activators, *in situ* ATR-IR and XANES/EXAFS investigations have been performed and are described below.

### *In situ* ATR-IR Measurements

The ATR-IR spectra of cyclohexane (CH), $Cr(acac)_3$ in CH and respective spectra measured after subsequent admixture of PNP and $AlMe_3$ are exemplarily shown in Figure 3a. For comparison, the spectra of $AlMe_3$ as well as PNP in CH are also included. The typical bands of $[acac]^-$ coordinated to the $Cr^{III}$ center appear at 1579 $cm^{-1}$ ($\nu$C=O), 1519 $cm^{-1}$ ($\nu_{as}$C–C–C), 1388/1352 $cm^{-1}$ ($\delta CH_3$) and 1274 $cm^{-1}$ ($\nu_s$C–C–C).[24] After adding the ligand, two new bands of PNP appear at 740 and 695 $cm^{-1}$ while all other bands do not change. This confirms our conclusion that there is no interaction between $Cr(acac)_3$ and PNP in the absence of an activator. However, after adding $AlMe_3$, the $Cr(acac)_3$ bands at 1579 and 1519 $cm^{-1}$ shift to higher wavenumbers. This points to a change of coordination of the $[acac]^-$ ligands. Bands at 1588 and 1526 $cm^{-1}$ were also observed for $Al(acac)_3$ solved in chloroform.[24b] Consequently, the observed shift might suggests a ligand exchange between $Cr(acac)_3$ and $AlMe_3$, leading to the formation of $Al(acac)_3$ which would also be in agreement with UV-vis results (Figure 2b). The $\delta CH_3$ bands of $AlMe_3$[25] at 768, 1197, 1375 $cm^{-1}$ shift and decrease strongly in the FTIR spectrum of the mixture of $Cr(acac)_3$, PNP and $AlMe_3$ (Figure 3a). This indicated a change of the coordination sphere of $AlMe_3$ by partial detachment and transfer of $CH_3$ to the Cr species (*vide infra*).

Unfortunately, it is not possible to study Cr–O or Cr-alkyl vibrations because the spectral region is not accessible with the ATR-IR probe.

A similar shift of the $Cr(acac)_3$ bands at 1579 and 1519 $cm^{-1}$ was also observed after adding other Al activators (Figure 3b), suggesting in all cases a ligand exchange between $Cr(acac)_3$ and activator followed by formation of $Al(acac)_3$.

### *In situ* XANES Results

XANES spectra of solid $Cr(acac)_3$ and $Cr(acac)_3$/PNP/activator solutions in cyclohexane are shown in Figure 4. The spectrum

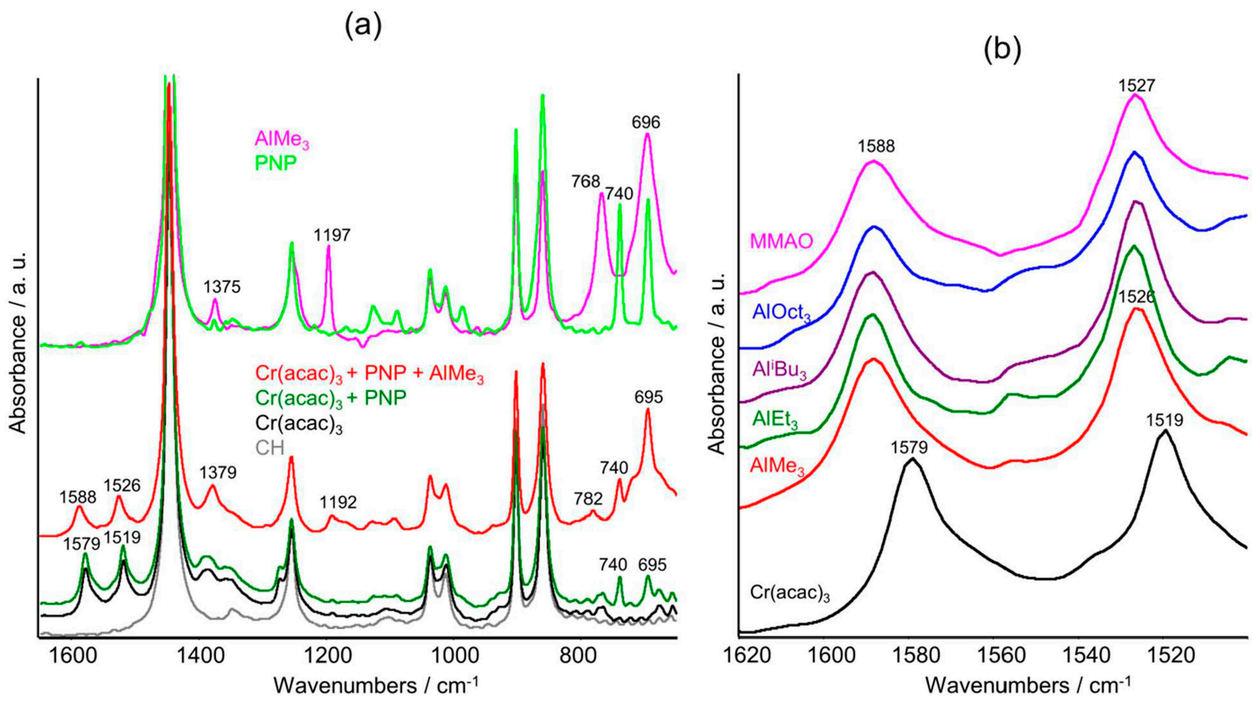


**Figure 3.** a) ATR-IR spectra of cyclohexane (CH), $Cr(acac)_3$ in CH and spectra measured after subsequent admixture of PNP and $AlMe_3$ (the spectra of $AlMe_3$ and PNP in CH are shown for comparison); b) normalized spectra of CH solutions containing $Cr(acac)_3$, PNP, and different activators.

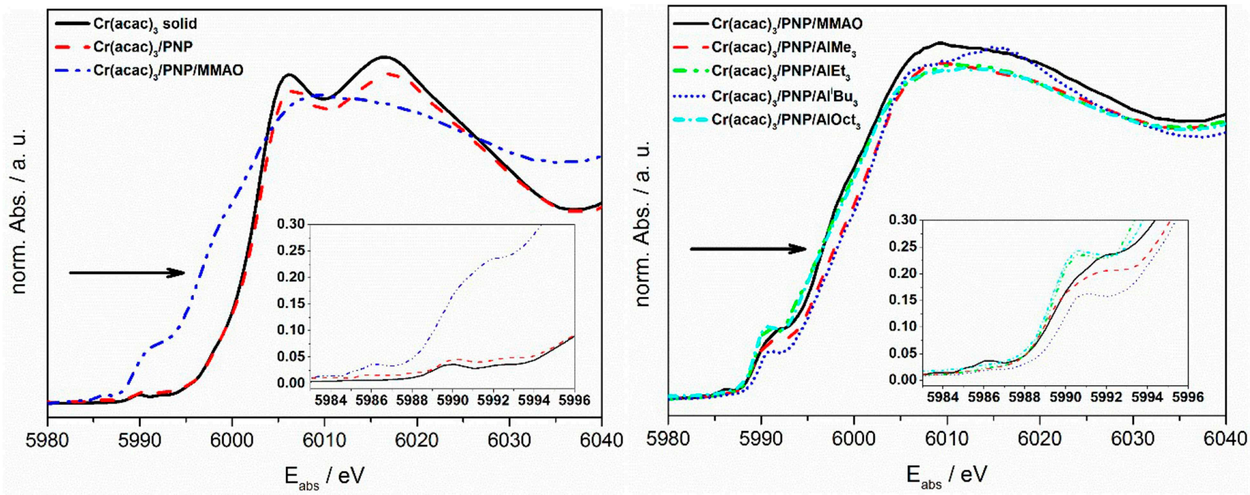


**Figure 4.** XANES spectra of the activation of $Cr(acac)_3$/PNP with MMAO (left) and in comparison to the other activators (right) in cyclohexane. Arrow indicates the half edge step. Inset: Enlarged pre-edge area. First derivative spectra are displayed in the supplementary information (Figure S6).

of the solid precursor $Cr(acac)_3$ is shown for comparison. The pre-edge region is characterized by a doublet signal at around 5991 and 5993 eV. Calculated density of states suggest that the former signal is caused by Cr(p+d) and O(p) states, while the later one is dominated by Cr(p) states. The low intensity of these signals originates from the octahedral symmetry at the $Cr^{III}$ center. The double peak feature in the white line is characteristic here for the 6-fold oxygen coordination as well. The spectrum after adding the PNP ligand to the $Cr(acac)_3$ solution without any activator is identical to the spectrum of pure $Cr(acac)_3$ and confirms, in agreement with UV-vis and FTIR data, that PNP ligand and Cr precursor do not interact in the absence of activator. When MMAO is added to the $Cr(acac)_3$/PNP solution, the intense double feature of the white line (6006.1 eV and 6016.5 eV), which is characteristic for the $[acac]^-$ ligand coordinated to Cr, vanishes. This is also true for the other $AlR_3$ activators except $Al^iBu_3$. In this case, a weak double peak structure is still visible. This may be an indication for a remaining $[acac]^-$ ligand at the Cr center, which is also supported by EXAFS data discussed below. Additionally, the structure and energy of the pre-edge peak changes upon adding the activators. Pure $Cr(acac)_3$ exhibits two weak pre-edge features at 5990.1 and 5992.6 eV. Since the prepeak represents a dipole forbidden 1 s→3d transition, only 3d→4p hybridization enables parity allowed transitions. In complexes with a symmetry center, such as in the octahedrally coordinated $Cr(acac)_3$, the prepeak intensity is usually much lower than in complexes without symmetry center. Solutions with PNP and MMAO or $AlMe_3$, for which a $Cr^I$ content of less than 2% was detected by EPR, are characterized by an intense shoulder at 5992.0 eV, indicating a reduced symmetry at the Cr center compared to $Cr(acac)_3$. A similar signature was identified by Botavina et al. as fingerprint of $Cr^{II}$, although at different energies due to a completely different chemical environment.[26] With the activators $AlEt_3$, $Al^iBu_3$ and $AlOct_3$ respectively, a $Cr^I$ fraction of 15–30% was determined via EPR. The corresponding XANES spectra show an increased splitting between the prepeak shoulder, now around 5990.5 eV, and the main edge (Table 2). Since the detection limit for a minor fraction in XANES spectra was estimated to 10% by Groppo et al.[27] it can thus be concluded that the prepeak shoulder at 5992.0 eV is the signature of $Cr^{II}$ in the present system. The shift of the prepeak shoulder to lower energies is in line with the expectations for a larger fraction of $Cr^I$. However, more detailed conclusions on changes of the Cr coordination in the presence of the different activators cannot be derived just based on the XANES data. This is only possible by EXAFS discussed below. The very weak prepeak at 5986 eV was assigned to a $Cr^{II}$ state as well by Groppo et al.[27–28] and can only be unequivocally observed for the activator MMAO.

Apart from the pre-edge feature, also the edge position changes upon adding different activators due to changes in the oxidation state. As pointed out by Groppo et al.,[27] chromium valence state determination from K-edge data is challenging, since the pre-edge and XANES region is very sensitive to the ligand environment, it is affected by the presence of different

**Table 2.** Energetic position of the pre-edge peak (PP) and edge position ($E_0$) determined by method 1 from the 2nd derivative of the spectra and by method 2 from the half edge step.

| Sample | PP [eV] | Meth. 1: $E_0$ [eV] (shift to $Cr(acac)_3$) | Meth. 2: $E_0$ [eV] (shift to $Cr(acac)_3$) |
|---|---|---|---|
| $Cr(acac)_3$ | 5990.1/ 5992.6 | 6005.1 | 6001.3 |
| $Cr(acac)_3$/PNP/ MMAO | 5986.0/ 5992.0 | 6003.6 (−1.5) | 5996.3 (−5.0) |
| $Cr(acac)_3$/PNP/ $AlMe_3$ | 5992.0 | 6004.9 (−0.2) | 5997.8 (−3.5) |
| $Cr(acac)_3$/PNP/$AlEt_3$ | 5990.5 | 6003.7 (−1.4) | 5996.3 (−5.0) |
| $Cr(acac)_3$/PNP/ $Al^iBu_3$ | 5986.5/ 5991.0 | 6005.0 (−0.1) | 5998.0 (−3.3) |
| $Cr(acac)_3$/PNP/ $AlOct_3$ | 5990.5 | 6004.1 (−1.0) | 5996.6 (−4.7) |

species that are averaged in the spectral signal.[10,29] It has thus to be emphasized here that the following discussion has to be considered under the basic assumption that a fraction of $Cr^{I}$ according to the EPR results is present, which manifest themselves in a systematic way in the pre-edge signals.

A number of different methods for determination of the edge position $E_0$ have been established.[29–30] Two of them were applied in this work to avoid misinterpretations. Method 1 described by Tromp et al.[29] uses the last edge contribution before the white line, which is determined from the second derivative of the spectrum. Method 2 takes the energy at values of 0.5 of the normalized absorption in the edge step as $E_0$. Both methods result in the same trend of shifts as indicated in Table 2. Method 1 results in an edge shift of maximum 2 eV between the $Cr^{III}$ precursor and the different $Cr(acac)_3$/PNP/activator solutions while method 2 shows a maximum edge shift of 5.0 eV between the activated solutions and the pure $Cr^{III}$ precursor.

In previous XAS studies of Cr catalyzed ethylene oligomerization it was found that the activated Cr species is in the divalent state.[3f,13b] The relevant energy found by method 1 for $Cr(acac)_3$/PNP/MMAO agrees with the value detected in ref. 13b confirming the approach and serving as reference value.[10] Taking into account the $Cr^{I}$ content of 2% with MMAO as activator obtained by EPR measurements, this sample can be considered to contain only $Cr^{II}$ species. All other samples, except for $AlMe_3$, contain higher fractions of $Cr^{I}$ and show lower activity and 1-octene selectivity and consequently these results confirm our previous results that identified $Cr^{II}$ as the active species. However, no unequivocal further correlation can be established between the edge shift, i.e. the average oxidation state and the observed activity and selectivity, and from the EPR detected $Cr^{I}$ content in comparison to the observed shifts it is deduced that ligand effects play an important role.

### *In situ* EXAFS Results

Structural differences have to be taken into account to explain the observed differences in the catalytic behavior. The local structure can be effectively probed by EXAFS spectroscopy. The results of the EXAFS analysis are summarized in Figure 5 and Table 3. The interpretation of these data is carried out in terms of a single, average structural model, which is assigned to a $Cr^{II}$ species. Due to the presence of 0% to 30% $Cr^{I}$ (Table 1), the proposed structures deduced from the structural parameters are subject to an error that increases from top to bottom in Table 3. This error is relativized by the fact that a part of this $Cr^{I}$ is not coordinated by the PNP ligand. By comparison of the small total percentage of $Cr^{I}$ (Table 1) with the relative EPR intensities of $Cr^{I}$ with and without PNP ligand (EPR signals at $g=2.0017$ and 1.998, respectively, Figure 1), it is obvious that there is essentially no $Cr^{I}$-PNP species with activators MMAO and $AlMe_3$ while the percentage of the former amounts to only $\approx 5\%$ for $AlEt_3$ and $\approx 15\%$ for $Al^{i}Bu_3$ and $AlOct_3$. Thus, an observed Cr–P pair can be reliably assigned to a $Cr^{II}$ species, even though in samples $Cr(acac)_3$/PNP/$Al^{i}Bu_3$ and $Cr(acac)_3$/PNP/$AlOct_3$ the $Cr^{II}$-P coordination number (Table 2) might be slightly underestimated since those systems contain also a minor percentage of $Cr^{I}$-PNP species. For the extreme case where $Cr^{I}$ is not coordinated by PNP at all (approached in fact with MMAO and $AlMe_3$), the largest possible Cr–P coordination number can be easily calculated. The respective values are given in Table 2 in parenthesis for activators $AlEt_3$, $Al^{i}Bu_3$ and $AlOct_3$.

Based on our previous study an initial model with two carbon atoms at $\approx 2.0$ Å, two phosphorus atoms at $\approx 2.4$ Å and one nitrogen neighbor at 2.8 Å has been applied as starting structure of the fitting procedure. Two further carbon shells at around 3.4–3.9 Å have to be included to achieve a satisfactory fit on unfiltered data. They do however not contain reliable structural information, as scattering from carbon shells mixes with multiple scattering signals at these distances. Conse-

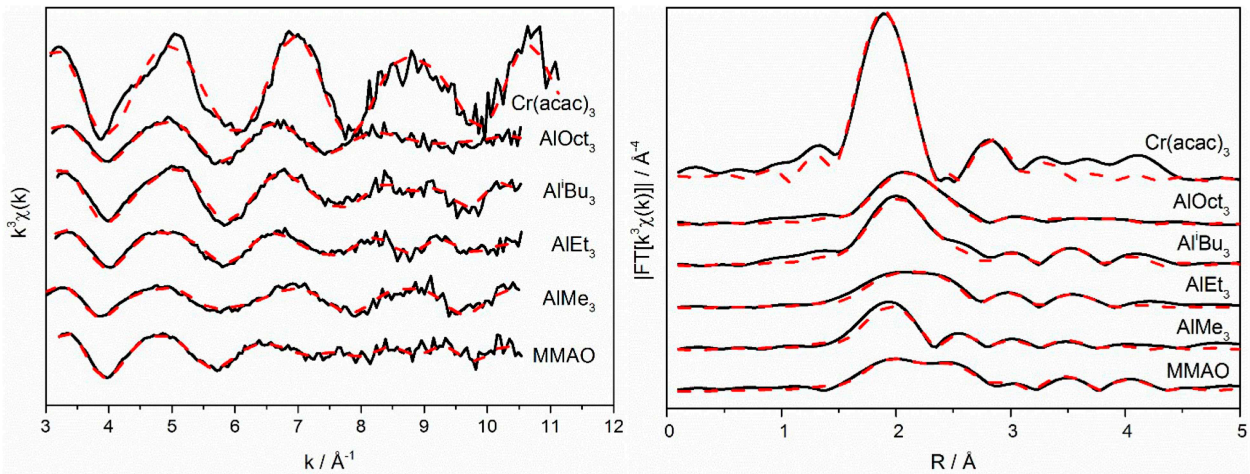


**Figure 5.** Experimental (solid lines) and calculated (dashed lines) $k^3\cdot\chi(k)$ (left) and Fourier transformed (right) EXAFS spectra of the different $Cr(acac)_3$/PNP/activator solutions. Imaginary parts are shown in Figure S7.

**Table 3.** Neighbor atoms, coordination numbers and distances derived by EXAFS analysis. An amplitude reduction factor of 0.8 as determined for the Cr $(acac)_3$ reference was used for all fits.

| Sample | Abs-Bs[a] | N(Bs)[b] | R(Abs-Bs)[c] [Å] | $\sigma^2 \cdot 10^4$ [d] [$Å^{-2}$] | R [e] [%] | Ef [f] [eV] |
|---|---|---|---|---|---|---|
| Solid $Cr(acac)_3$ | Cr–O | *6* | 1.96±0.02 | 6.0±0.6 | 26.7 | 5.90 |
| | Cr–C | *6* | 2.91±0.03 | 9.0±0.9 | | |
| | Cr–C | *3* | 3.18±0.03 | 2.0±0.2 | | |
| $Cr(acac)_3$/ | Cr–C | 2.0±0.2 | 2.03±0.02 | 7.0±0.7 | 22.3 | 10.45 |
| PNP/ | Cr–P | 2.1±0.2 | 2.38±0.02 | 22.0±2.2 | | |
| MMAO | Cr–N[h] | 1.7±0.2 | 2.80±0.03 | 25.0±2.5 | | |
| $Cr(acac)_3$/ | Cr–C | 2.6±0.3 | 2.04±0.02 | 2.0±0.2 | 28.5 | 7.21 |
| PNP/$AlMe_3$ | Cr–C | 0.9±0.1 | 2.29±0.02 | 2.0±0.2 | | |
| | Cr–C | 2.3±0.2 | 2.83±0.03 | 25.0±2.5 | | |
| $Cr(acac)_3$/ | Cr–C | 2.1±0.2 | 2.04±0.02 | 3.0±0.3 | 22.9 | 8.70 |
| PNP/$AlEt_3$ | Cr–P | 1.0±0.1 (1.17[g]) | 2.36±0.02 | 5.0±0.5 | | |
| | Cr–N[h] | 1.0±0.1 | 2.91±0.03 | 3.0±0.3 | | |
| $Cr(acac)_3$/ | Cr–C | 3.5±0.4 | 2.03±0.02 | 2.0±0.2 | 24.0 | 8.54 |
| PNP/$Al^iBu_3$ | Cr–P | 1.0±0.1 (1.38[g]) | 2.34±0.02 | 8.0±0.8 | | |
| | Cr–N[h] | 0.5±0.1 | 2.97±0.03 | 2.0±0.2 | | |
| $Cr(acac)_3$/ | Cr–C | 2.2±0.2 | 2.05±0.02 | 2.0±0.2 | 22.0 | 8.95 |
| PNP/$AlOct_3$ | Cr–P | 1.5±0.2 (2.14[g]) | 2.34±0.02 | 13.0±1.3 | | |
| | Cr–N[h] | 0.7±0.1 | 2.92±0.03 | 16.0±1.6 | | |

All values are averaged values of k-weighting k=1–3. [a] Abs=X-ray absorbing atom, Bs=backscattering atom, [b] Number of backscattering atoms, [c] Distance of absorbing atom to backscattering atom, [d] Debye-Waller-like factor, [e] Fit-index, [f] Fermi energy, that accounts for the shift between theory and experiment, [g] Numerically obtained maximal coordination number, assuming the extreme case where no $Cr^I$ is coordinated by the PNP ligand, [h] Although carbon and nitrogen cannot be distinguished in the EXAFS analysis, this shell is denoted as Cr–N, as the presence of a Cr–P shell makes a Cr–N contribution very plausible.

quently, they are not shown in Table 3, but in the Supporting Information.

For the known system $Cr(acac)_3$/PNP/MMAO, distances and coordination numbers agree very well with our previous study.[10] Together with the XANES data, the formation of a $(PNP)Cr^{II}(CH_3)_2$ complex as active species could therefore be confirmed here as well. The increased Debye-Waller factor in the present study is caused by the very high noise level due to the very low chromium concentration and the experimental conditions. Generally, the appearance of rather high Debye-Waller factors is correlated to low chromium concentrations and signal-to-noise ratios in the experimental data. In the presence of the $AlMe_3$ activator, a completely different structure is found. First attempts to adjust a Cr–P shell resulted in a coordination number of 0.3, which is statistically not significant. Instead, the superior fit, given in Table 3, reflects full methylation of the Cr center resulting in a $[Cr(CH_3)_n]^{(n-2)-}$ complex with n $\approx$ 4. Hence a third Cr–C shell was fitted instead of Cr–N found in all other fits. This shell increased the quality of fit substantially and can indeed only be due to multiple scattering effects. The effective methylation by $AlMe_3$[5b,23] thus prevents coordination of the PNP ligand.

Due to the presence of minor fractions of $Cr^I$ for the activation with $AlEt_3$, $AlOct_3$ and $Al^iBu_3$ a single-model fit is prone to a large error and Debye-Waller like factors due to averaging effects, in particular for the case of $AlOct_3$. Nevertheless, since no defined model for the $Cr^I$ species exists so far, a two-model fit could not be carried out in terms of a path-by-path analysis. Instead a shell-by-shell fit in terms of radial distribution functions is used here which is better suited for solution investigations of unknown species.

The obtained results for systems containing $AlEt_3$ and $AlOct_3$ are very similar. In both cases, Cr is coordinated by around two carbon atoms. In contrast to the MMAO system, fit results are consistent with coordination of one P atom of the PNP ligand at the Cr center. If the numerically obtained maximal $Cr^{II}$-P value is considered, the coordination of the second phosphine appears to be possible in case of $AlOct_3$ but not for $AlEt_3$. Furthermore, the number of Cr–N bonds is reduced and the Cr–N distance is elongated in both systems. This may suggest that the larger alkyl groups at least partially hinder the complete coordination of the PNP ligand to form a chelate complex.

For the activation with $Al^iBu_3$ the resulting fit model is quite different. The first coordination sphere at $\approx$ 2.0 Å consists of 3.5±0.4 carbon atoms, which is almost twice the value of the MMAO system. As for $AlEt_3$ and $AlOct_3$, only one phosphorus atom is coordinated to Cr with a slightly shortened Cr–P distance compared to MMAO. Even if the Cr–P coordination number is corrected for the $Cr^I$ content, still only one phosphorous ligand is coordinated to Cr within the error bar.

Additionally, the number of coordinated nitrogen atoms at 2.97 Å is almost zero and the Cr–N distance increased further compared to the $AlEt_3$ and $AlOct_3$ systems. XANES data (Figure 4) presented above show some remaining double peak XANES feature characteristic for $Cr(acac)_3$. Considering the fact that Cr–C and Cr–O bonds cannot be distinguished by EXAFS, the obtained coordination numbers can thus be interpreted by a mixture of Cr-*iso*-butyl, Cr-acac and Cr-phosphine species.

### Structure-Reactivity Relationships

Based on combined evaluation of all spectroscopic results, a structure-activity correlation can be obtained. The structure of the Cr complex, which is formed in cyclohexane upon mixing the $Cr(acac)_3$ precursor with the $Ph_2PN(^iPr)PPh_2$ ligand and the different activators is shown in Figure 6. We like to stress here that these structures are the conclusion of the combined spectroscopic approach by UV-vis, ATR-IR and XAS under consideration of the individual methodical limitations. As mentioned in the EXAFS part, the potential error is increasing in Figure 6 from top to bottom. Nevertheless, the structural trend is very clear, presenting proposals for highly active, medium active and inactive structures: No reaction occurs between Cr $(acac)_3$ and PNP in the absence of any ligand. The addition of all activators except $AlMe_3$ enable coordination of PNP to the Cr center, yet only with MMAO a bidentate coordination by two P atoms is observed while in the presence of $AlR_3$ (R = Et, $^iBu$ or Oct) PNP coordinates only *via* one P atom. Most probably, alkylation of the Cr center by the activator and coordination of PNP compete with each other for the saturation of vacant positions created by detachment of $[acac]^-$ from the Cr center. In the presence of a very effective alkylating agent such as $AlMe_3$, complete methylation is observed. With increasing length and/or branching of the alkyl groups transferred from the activator to the Cr center, monodentate coordination of PNP is deduced from the EXAFS results, probably due to steric reasons. Decrease of the alkylation rate with rising length of the alkyl rest in the order methyl > ethyl > allyl > propyl > butyl has also been found in other alkylation reactions.[31] This may be a reason why with the branched $Al^iBu_3$ activator complete substitution of $[acac]^-$ is not possible. Replacement of $[acac]^-$ by PNP and/or alkyl groups is indeed only possible with reduction of the Cr center. This is evident from both XAS and EPR spectroscopy, whereby EPR detects selectively $Cr^I$ while XAS reflects the average chromium valence state. Negligible amounts of $Cr^I$ were measured with both MMAO and $AlMe_3$ and the $(PNP)Cr(CH_3)_2$ complex identified by EXAFS in the presence of MMAO implies that Cr is divalent. Since the variations of the XANES edge energies are comparatively small, the chromium valence state of the major fraction is two in all cases. The differences in the Cr coordination found by EXAFS and the different fractions of $Cr^I$ in the presence of $AlR_3$ are then responsible for the variations of the edge energies. Reduction to $Cr^I$ that is supposed to be catalytically inactive,[10] is negligible for the methylating activators $AlMe_3$ and MMAO. It increases in the order $AlEt_3 < Al^iBu_3 \approx AlOct_3$ with increasing chain length and branching of the alkyl rest, which hinders fast coordination of PNP. On the other hand, it is known that chelating by PNP prevents deep reduction of Cr.[18] Thus, it is easy to understand that not only the total $Cr^I$ content but also the percentage of PNP-containing $Cr^I$ increases with rising chain length/branching of the alkyl rest, since only monodentate coordination of PNP could be realized in the latter cases.

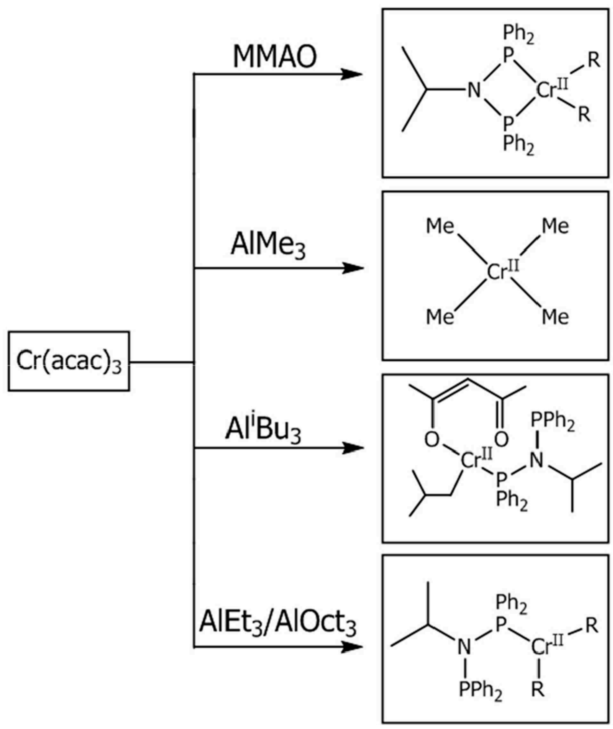


**Figure 6.** Proposed structure of complexes formed *in situ* from $Cr(acac)_3$, $Ph_2PN(^iPr)PPh_2$ and different activators (formal charges are omitted for clarity).

Comparison of the proposed structure of the *in situ* formed Cr complexes (Figure 6) with the catalytic performance (Table 1) suggests the following relations: Superior performance with highest productivity of 1-octene and suppressed formation of shorter chain products with MMAO as activator is achieved when the PNP ligand binds to a $Cr^{II}$ center in a bidentate way *via* two P atoms to form a proper chelate complex. Together with the two additional $CH_3$ ligands, an optimum steric configuration is formed. This stabilizes the chromacycle intermediate (Scheme 1) assumed to be formed upon subsequent attachment of ethylene to the $(PNP)Cr^{II}(CH_3)_2$ species from which 1-octene is liberated.[3d,10,32] This is obviously not possible at all, when the PNP ligand does not coordinate to Cr (with $AlMe_3$). In this case, only short chain products with less than 6 C

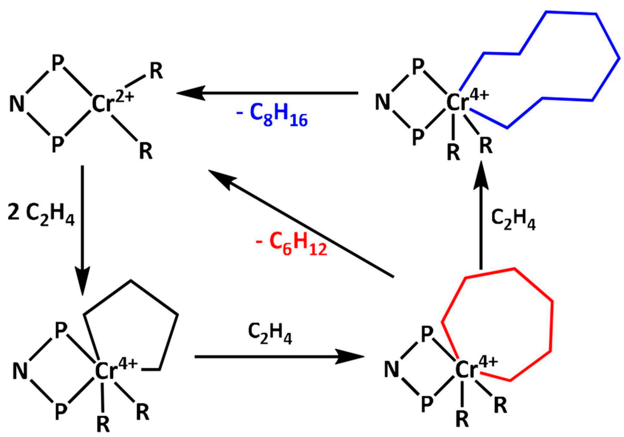


**Scheme 1.** Metallacycle mechanism for the selective tri- and tetramerization of ethylene.[3d]

atoms are formed. Monodentate coordination of PNP (with $AlEt_3$, $Al^iBu_3$ and $AlOct_3$) raises the percentage of 1-hexene at the expense of $C_{<6}$ products, yet this beneficial effect is weakened with rising chain length/branching of the alkyl rest which may cause steric hindrance for the formation of the chromacycle intermediate. In the case of $AlOct_3$ with the longest alkyl rest even the formation of long polymer chains is favored.

On the other hand, decreasing alkylation rates with rising bulkiness of the alkyl rests seem to promote deep reduction to $Cr^I$. However, compared to proper bidentate coordination of PNP, this effect seems to be less important for catalytic performance, since ethylene consumption with $AlEt_3$ and $Al^iBu_3$ is the same and even slightly higher with $AlOct_3$ although the $Cr^I$ percentage increases in the order $15\% < 28\% < 30\%$ (Table 1).

## Conclusions

By exhaustive combination of the complementary spectroscopic techniques IR, UV-vis, and in particular EPR and XAS new insights into the effect of the activator on the active species formed for ethylene oligomerization could be gained. All applied spectroscopic techniques confirm consistently that no coordination of the $Ph_2PN(^iPr)PPh_2$ ligand to the $Cr(acac)_3$ precursor occurs in the absence of activator. In the activation process, the PNP ligand and the alkyl groups of the activator compete with each other for occupation of the vacant positions created by release of the $[acac]^-$ ligands. In agreement with literature data,[31a] alkylation was found to be fastest with methyl moieties of $AlMe_3$ which forms a per-methylated chromium center preventing coordination of PNP. Consequently, with this activator no $C_{>5}$ products are formed. Bidentate coordination of the ligand to form a PNP–Cr chelate complex is of utmost importance for maximum 1-octene productivity, which is achieved only with MMAO. Rising bulkiness of the alkyl rests due to higher chain length and/or branching leads to coordination of the PNP ligand to Cr by only one P atom with no chelate complex formed. In these cases 1-hexene is the major product besides significant amounts of shorter chain products. This may be due to steric constraints imposed by the bulkier alkyl rests and/or the less rigid dangling fixation of PNP at the Cr center that hinders formation of a chromacycle intermediate from which 1-octene can be selectively liberated.

With all activators tested, the initial $Cr^{III}$ in the precursor is reduced to $Cr^{II}$ which is considered to be part of the active $Cr^{II}$/$Cr^{IV}$ redox cycle, in agreement with previous results.[3a,4,10,33] Deeper reduction to $Cr^I$ occurs with rising bulkiness of the alkyl rests in the activators, reaching 30% for $AlOct_3$. However, this appeared to be not important for catalytic performance compared to the tremendous impact of PNP coordination.

## Acknowledgment

*The Deutsche Forschungsgemeinschaft (DFG) is acknowledged for funding (grant numbers BA 4467/4-1 and BR 1380/23-1). We thank PETRA III (Hamburg, Germany) for provision of beamtime and support during the measurements by Dr. Edmund Welter.*

## Conflict of Interest

The authors declare no conflict of interest.

**Keywords:** aluminium activators · chromium complexes · ethylene tetramerization · *in situ* XANES/EXAFS · *operando* EPR spectroscopy

[1] a) J. Skupinska, *Chem. Rev.* **1991**, *91*, 613–648; b) L. H. Do, J. A. Labinger, J. E. Bercaw, *Organometallics* **2012**, *31*, 5143–5149.
[2] W. Keim, *Angew. Chem. Int. Ed. Engl.* **2013**, *52*, 12492–12496.
[3] a) K. A. Alferov, G. P. Belov, Y. Meng, *Appl. Catal. A* **2017**, *542*, 71–124; b) P. W. N. M. van Leeuwen, N. D. Clément, M. J. L. Tschan, *Coord. Chem. Rev.* **2011**, *255*, 1499–1517; c) D. F. Wass, *Dalton Trans.* **2007**, 816–819; d) M. J. Overett, K. Blann, A. Bollmann, J. T. Dixon, D. Haasbroek, E. Killian, H. Maumela, D. S. McGuinness, D. H. Morgan, *J. Am. Chem. Soc.* **2005**, *127*, 10723–10730; e) A. Bollmann, K. Blann, J. T. Dixon, F. M. Hess, E. Killian, H. Maumela, D. S. McGuinness, D. H. Morgan, A. Neveling, S. Otto, M. Overett, A. M. Z. Slawin, P. Wasserscheid, S. Kuhlmann, *J. Am. Chem. Soc.* **2004**, *126*, 14712–14713; f) K. Blann, A. Bollmann, H. de Bod, J. T. Dixon, E. Killian, P. Nongodlwana, M. C. Maumela, H. Maumela, A. E. McConnell, D. H. Morgan, M. J. Overett, M. Prétorius, S. Kuhlmann, P. Wasserscheid, *J. Catal.* **2007**, *249*, 244–249.
[4] J. T. Dixon, M. J. Green, F. M. Hess, D. H. Morgan, *J. Organomet. Chem.* **2004**, *689*, 3641–3668.
[5] a) S. Peitz, B. R. Aluri, N. Peulecke, B. H. Mueller, A. Woehl, W. Mueller, M. H. Al-Hazmi, F. M. Mosa, U. Rosenthal, *Chem. Eur. J.* **2010**, *16*, 7670–7676; b) E. H. Kim, H. M. Lee, M. S. Jeong, J. Y. Ryu, J. Lee, B. Y. Lee, *ACS Omega* **2017**, *2*, 765–773; c) X. Ji, L. Song, C. Zhang, J. Jiao, J. Zhang, *Inorg. Chim. Acta* **2017**, *466*, 117–121; d) Y. Yang, Z. Liu, B. Liu, R. Duchateau, *ACS Catal.* **2013**, *3*, 2353–2361; e) A. Jabri, C. B. Mason, Y. Sim, S. Gambarotta, T. J. Burchell, R. Duchateau, *Angew. Chem. Int. Ed.* **2008**, *47*, 9717–9721; *Angew. Chem.* **2008**, *120*, 9863–9867.
[6] a) A. J. Rucklidge, D. S. McGuinness, R. P. Tooze, A. M. Z. Slawin, J. D. A. Pelletier, M. J. Hanton, P. B. Webb, *Organometallics* **2007**, *26*, 2782–2787; b) W. Janse van Rensburg, J.-A. van den Berg, P. J. Steynberg, *Organometallics* **2007**, *26*, 1000–1013.
[7] D. S. McGuinness, D. B. Brown, R. P. Tooze, F. M. Hess, J. T. Dixon, A. M. Z. Slawin, *Organometallics* **2006**, *25*, 3605–3610.
[8] A. Jabri, P. Crewdson, S. Gambarotta, I. Korobkov, R. Duchateau, *Organometallics* **2006**, *25*, 715–718.
[9] a) A. Jabri, C. Temple, P. Crewdson, S. Gambarotta, I. Korobkov, R. Duchateau, *J. Am. Chem. Soc.* **2006**, *128*, 9238–9247; b) C. Temple, A. Jabri, P. Crewdson, S. Gambarotta, I. Korobkov, R. Duchateau, *Angew. Chem. Int. Ed. Engl.* **2006**, *45*, 7050–7053.
[10] J. Rabeah, M. Bauer, W. Baumann, A. E. C. McConnell, W. F. Gabrielli, P. B. Webb, D. Selent, A. Brückner, *ACS Catal.* **2013**, *3*, 95–102.
[11] G. P. Belov, *Pet. Chem.* **2012**, *52*, 139–154.
[12] T. K. Han, M. A. Ok, S. S. Chae, S. O. Kang, J. H. Jung, *US Patent 2010/0137669 A1*, US, **2010**.
[13] a) T. S. Ertel, H. Bertagnolli, S. Hückmann, U. Kolb, D. Peter, *Appl. Spectrosc.* **1992**, *46*, 690–698; b) B. Ravel, M. Newville, *J. Synchrotron Radiat.* **2005**, *12*, 537–541; c) M. Newville, *J. Synchrotron Radiat.* **2001**, *8*, 322–324; d) M. Newville, P. Līviņš, Y. Yacoby, J. J. Rehr, E. A. Stern, *Phys. Rev. B* **1993**, *47*, 14126–14131.
[14] N. Binsted, S. S. Hasnain, *J. Synchrotron Radiat.* **1996**, *3*, 185–196.
[15] a) E. A. Stern, *Phys. Rev. B* **1993**, *48*, 9825–9827; b) M. Bauer, H. Bertagnolli, *J. Phys. Chem. B* **2007**, *111*, 13756–13764.
[16] N. Binsted, R. W. Strange, S. S. Hasnain, *Biochemistry* **1992**, *31*, 12117–12125.

[17] D. C. Koningsberger, B. L. Mojet, G. E. van Dorssen, D. E. Ramaker, *Top. Catal.* **2000**, *10*, 143–155.
[18] A. Brückner, J. K. Jabor, A. E. C. McConnell, P. B. Webb, *Organometallics* **2008**, *27*, 3849–3856.
[19] A. M. Lifschitz, N. A. Hirscher, H. B. Lee, J. A. Buss, T. Agapie, *Organometallics* **2017**, *36*, 1640–1648.
[20] F. F. Karbach, J. R. Severn, R. Duchateau, *ACS Catal.* **2015**, *5*, 5068–5076.
[21] a) R. H. Holm, F. A. Cotton, *J. Am. Chem. Soc.* **1958**, *80*, 5658–5663; b) A. Gairola, G. V. Kunte, D. Chopra, T. N. G. Row, A. M. Umarji, S. A. Shivashankar, *Polyhedron* **2010**, *29*, 2680–2688.
[22] a) J. N. Schrauben, Michigan State University **2010**; b) W. Schmidt, J. H. Swinehart, H. Taube, *J. Am. Chem. Soc.* **1971**, *93*, 1117–1123.
[23] S. Horvath, S. I. Gorelsky, S. Gambarotta, I. Korobkov, *Angew. Chem. Int. Ed.* **2008**, *47*, 9937–9940; *Angew. Chem.* **2008**, *120*, 10085–10088.
[24] a) E. Tarcan, *J. Macromol. Sci., Part B:* **2015**, *54*, 897–906; b) R. Larsson, O. Eskilsson, S. Svensson, T. Holme, A. A. Lindberg, G. Jansen, B. Lamm, B. Samuelsson, *Acta Chem. Scand.* **1969**, *23*,1765-1779.
[25] S. Pinchas, B. L. Silver, I. Laulicht, *J. Chem. Phys.* **1967**, *46*, 1506–1510.
[26] M. Botavina, C. Barzan, A. Piovano, L. Braglia, G. Agostini, G. Martra, E. Groppo, *Catal. Sci. Technol.* **2017**, *7*, 1690–1700.
[27] E. Groppo, G. A. Martino, A. Piovano, C. Barzan, *ACS Catal.* **2018**, *8*, 10846–10863.
[28] D. Gianolio, E. Groppo, J. G. Vitillo, A. Damin, S. Bordiga, A. Zecchina, C. Lamberti, *Chem. Commun.* **2010**, *46*, 976–978.
[29] M. Tromp, J. Moulin, G. Reid, J. Evans, *AIP Conf. Proc.* **2007**, Medium: X; 699–701.
[30] a) T. W. Capehart, J. F. Herbst, R. K. Mishra, F. E. Pinkerton, *Phys. Rev. B* **1995**, *52*, 7907–7914; b) G. Bunker, *Introduction to XAFS: A Practical Guide to X-ray Absorption Fine Structure Spectroscopy*, Cambridge University Press, Cambridge **2010**.
[31] a) J. A. Manso, M. T. Pérez-Prior, M. d. P. García-Santos, E. Calle, J. Casado, *Chem. Res. Toxicol.* **2005**, *18*, 1161–1166; b) D. Gong, W. Liu, T. Chen, Z. R. Chen, K. W. Huang, *J. Mol. Catal. A* **2014**, *395*, 100–107.
[32] a) A. Bollmann, K. Blann, J. T. Dixon, F. M. Hess, E. Killian, H. Maumela, D. H. Morgan, A. Neveling, S. Otto, M. Overett, D. S. McGuinness, A. M. Z. Slawin, *Vol. 229*, 1 ed., **2005**, pp. 930; b) T. Gunasekara, J. Kim, A. Preston, D. K. Steelman, G. A. Medvedev, W. N. Delgass, O. L. Sydora, J. M. Caruthers, M. M. Abu-Omar, *ACS Catal.* **2018**, 6810–6819; c) S. Kuhlmann, K. Blann, A. Bollmann, J. T. Dixon, E. Killian, M. C. Maumela, H. Maumela, D. H. Morgan, M. Pretorius, N. Taccardi, P. Wasserscheid, *J. Catal.* **2007**, *245*, 279–284; d) T. Agapie, S. J. Schofer, J. A. Labinger, J. E. Bercaw, *J. Am. Chem. Soc.* **2004**, *126*, 1304–1305.
[33] T. Agapie, *Coord. Chem. Rev.* **2011**, *255*, 861–880.

Manuscript received: August 7, 2019
Revised manuscript received: October 22, 2019
Accepted manuscript online: October 23, 2019
Version of record online: December 11, 2019

 